

AnyRotate: Gravity-Invariant In-Hand Object Rotation with Sim-to-Real Touch

Max Yang¹, Chenghua Lu¹, Alex Church^{2†}, Yijiong Lin¹, Chris Ford¹, Haoran Li¹,
Efi Psomopoulou¹, David A.W. Barton^{1*}, Nathan F. Lepora^{1*}

¹University of Bristol

²Cambrian Robotics

<https://maxyang27896.github.io/anyrotate/>

Abstract—In-hand manipulation is an integral component of human dexterity. Our hands rely on tactile feedback for stable and reactive motions to ensure objects do not slip away unintentionally during manipulation. For a robot hand, this level of dexterity requires extracting and utilizing rich contact information for precise motor control. In this paper, we present AnyRotate, a system for gravity-invariant multi-axis in-hand object rotation using dense featured sim-to-real touch. We construct a continuous contact feature representation to provide tactile feedback for training a policy in simulation and introduce an approach to perform zero-shot policy transfer by training an observation model to bridge the sim-to-real gap. Our experiments highlight the benefit of detailed contact information when handling objects with varying properties. In the real world, we demonstrate successful sim-to-real transfer of the dense tactile policy, generalizing to a diverse range of objects for various rotation axes and hand directions and outperforming other forms of low-dimensional touch. Interestingly, despite not having explicit slip detection, rich multi-fingered tactile sensing can implicitly detect object movement within grasp and provide a reactive behavior that improves the robustness of the policy, highlighting the importance of information-rich tactile sensing for in-hand manipulation.

I. INTRODUCTION

The dexterity of the human hand is a fundamental capability we rely on in everyday activities. This versatility of manipulating objects of varying shapes and sizes has likewise been a long-standing goal for robot manipulation [43]. In-hand manipulation refers to the ability to reposition and reorient objects by re-grasping or finger gaiting, where contacts with the object must be detached and re-positioned locally during manipulation [7]. These tasks can be hugely challenging with robot hands due to the high degree of actuation, fine motor control, and large environment uncertainties. While significant advances have been made in recent years, most prominently the work by OpenAI [2, 5], they have primarily relied on vision-based systems which are not necessarily well suited to this task due to significant self-occlusion. Overcoming these issues often requires multiple cameras and complicated setups that are not representative of natural embodiment.

More recently, researchers have begun to explore the in-hand object rotation problem with proprioception and touch

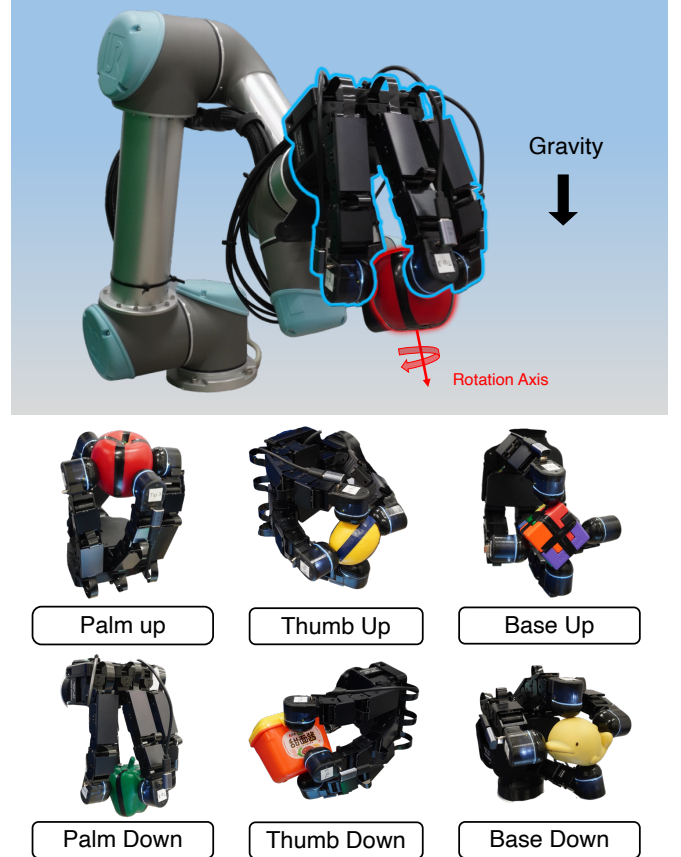


Fig. 1: Setup: A 4-fingered 16-DoF tactile robot hand attached to a UR5 performing in-hand object rotation (*top*), experimented in six key hand orientations with respect to gravity: palm up, palm down, thumb up, thumb down, base up and base down (*bottom*).

sensing without vision [27, 47]. A representative task of in-hand manipulation involves continuous object rotation about a desired axis while the object is grasped. A general formulation of this problem could result in a policy capable of object rotation about any chosen rotation axis in any hand orientation, which is particularly advantageous when the hand can move to any orientation in 3D space. However, this can be a difficult task to achieve as it requires high-precision control and comprehension of complex interaction physics that cannot be visually observed: any finger misplacement can induce slip and lead to irreversible states. The challenge is further complicated by the gravitational loading of the fingers which

* These authors contributed equally.

† Work done while at University of Bristol.

Correspondence to max.yang@bristol.ac.uk

can significantly influence fingertip actuation. This has led to previous work being limited to rotating about the primary axes and fixing the hand to a single orientation [48, 62].

Touch is expected to play an essential role as it allows the capture of detailed contact information to better control the robot-object interaction. Vision-based tactile sensors have become increasingly popular, *e.g.* the GelSight or TacTip sensors [63, 59], partly due to their affordability and compactness. They can also provide precise and detailed spatial information about the contact through high-resolution tactile images. However, this rich tactile information has not yet been fully exploited for in-hand dexterous manipulation. Previous studies have reduced the high-resolution tactile images to low-dimensional, binary, or discretized representations [48, 28]. While such approaches may reduce the sim-to-real gap, they also lose contact information. One might expect that a more detailed tactile representation could improve the performance and enable new tasks, which is explored in this work.

In this paper, we introduce AnyRotate: a robot system for performing multi-axis gravity-invariant in-hand object rotation with dense featured sim-to-real touch. Here, we propose to tackle this challenge with a goal-conditioned RL formulation and precision grasp manipulation. We present a new fingertip-like soft biomimetic optical tactile sensor based on the DigiTac [33] version of the TacTip, which has a compact design with a large curved sensing area that is well suited for dexterous manipulation. Prior work with the DigiTac/TacTip has shown its ability to accurately predict and use contact pose information for servo control, which can also be applied to sim-to-real reinforcement learning (RL) for learning complex control policies [61]. We extend this sim-to-real approach by simultaneously predicting continuous contact pose and contact force readings, features that can be critical for precise manipulation under noisy conditions. In the real world, we mount these sensors onto the fingertips of an Allegro four-fingered fully-actuated robot hand and leverage information in the full tactile image to provide rich tactile feedback for performing stable in-hand object rotation.

Our principal contributions for precision grasp manipulation with a fully-actuated 4-fingered robot hand are, in summary:

- 1) We develop an RL formulation using auxiliary goals and adaptive curriculum to achieve sample-efficient training of a unified policy, capable of in-hand object rotation about any chosen rotation axis in any hand direction.
- 2) We introduce a dense tactile representation and highlight the benefit of acquiring more detailed contact information over binary or discretized representations for manipulating a range of unseen objects with various geometries and properties.
- 3) We present a feature extraction method to achieve zero-shot sim-to-real transfer of our tactile policy. We validate our methods in the real world on 10 diverse objects and demonstrate strong robustness when rotating in various hand directions and about different rotation axes.

All software and hardware required to reproduce the experiments in this paper will be made available as open-source repositories with documentation on their use.

II. RELATED WORK

Dexterous Manipulation: Due to the complexity of the contact physics in dexterous manipulation, work on this topic has traditionally relied on planning and control using simplified models [21, 22, 8, 50, 19, 34, 46, 51]. With improved hardware and design, these methods have continued to demonstrate an increased level of dexterity. [6, 53, 57, 18, 56, 40, 26, 20, 44]. While these methods offer performance guarantees, they are often limited by the underlying assumptions. With the advance of machine learning, learning-based control has become a popular approach to achieving dexterity [5, 2, 41, 23, 12, 48, 24]. However, the majority of prior works use vision as the primary sense for object manipulation, either directly learning from visual images [11] or indirectly through extracted low-dimensional features [3]. This requires accurately tracking the pose of an object in a highly dynamic scene and any occlusions could lead to a drop in performance. More recently, researchers have proposed using proprioception [55, 49, 45] and binary contact data to perform in-hand object rotation [28, 62]. However, these implicit or low-dimensional tactile data do not capture detailed contact information which may be more advantageous for higher precision control and manipulation.

The work most closely related to ours is by Qi et al. [47] on a proprioception system to perform in-hand object rotation via stable precision grasping, also using the Allegro hand. This was further extended in [48], which leveraged vision and touch to perform multi-axis object rotation for a larger object set. However, these studies were limited to policies that could rotate objects about a single axis or primary axes, and rotation was achieved with the object resting on the domed fingertips in a fixed palm-up hand orientation. In addition, touch sensing was confined to discretized contact locations, which limits the contact information. Compared to their work, we present a tactile-only method for a more general in-hand rotation problem around any axis and hand orientation where the object needs to be securely grasped, along with considering more general dense and continuous tactile representations to study the importance of this modality.

Sim-to-real Tactile Sensing: Learning in simulation has been increasingly exploited in the field of robot learning due to efficiency and safety. This is especially true in tactile robotics where the sensors are continuously interacting with the environment and can potentially be damaged [1, 32]. Therefore, simulation and sim-to-real techniques have been critical tools in tactile robotics research. While we focus on vision-based tactile sensing; an overview of simulation for other sensors is covered in [42]. Various methods have been proposed to simulate high-fidelity tactile images [17, 58, 54, 15], and in accordance different tactile sim-to-real approaches have been developed [16, 25, 14, 60, 37]. Xu et al. leveraged a differentiable simulation to approximate the contact force field applied to a tactile sensor [60]. However, their method required complicated contact modeling and was limited to a flat rigid sensor. Several works have proposed high-frequency rendering

of tactile images using depth and have shown its feasibility for sim-to-real RL [16, 35, 36]. However, learning an RL policy using tactile images can be computationally expensive and inefficient, especially for a highly parallelized simulator. In this paper, we extend the work by Yang et al. [61] and leverage explicit contact features in IsaacGym [39] to represent the tactile information obtained from a vision-based tactile sensor. This provides a more efficient representation for training RL policies with tactile feedback.

III. SYSTEM SETUP

A. Real-world Setup

In our real-world setup, we use a 16-DoF Allegro Hand with customized tactile sensors attached to each of its fingertips. This design of the sensor is based on the DigiTac version [33] of the TacTip [59, 32], a soft optical tactile sensor that provides contact information through pin motion under its sensing surface. The DigiTac has a TacTip skin replacing the GelSight skin of the Meta DIGIT sensor [30]; however, here we have redesigned the DIGIT base to be more compact with a new PCB board, modular camera and lighting system (Fig. 2). Specifically, we redesigned the tactile sensor to fit seamlessly as fingertips for the Allegro Hand, and improved the morphology of the skin and base connector to provide a larger and smoother sensing surface for greater fingertip dexterity. The tactile sensor skin and base are entirely 3D printed with Agilus 30 for skin and vero-series for the pin tips and casings. Each base contains a custom camera driver board (with the OV5693 camera, 120° view) built on the SPCA2650A chipset, which connects to the computer via a USB cable. The output can be streamed asynchronously at a frame rate of 30FPS, which is sufficient for our task. We perform post-processing using OpenCV [9] in real-time. As the tactile fingertips are primarily sensorized over a front-facing area, we experimented with their orientation relative to the fingers and tried to maximize contact sensing during in-hand object rotation. We placed the tactile fingertips with the offsets shown in Fig. 2. Simultaneously, the Allegro Hand is controlled asynchronously by a torque PD controller at 300 Hz. The sampling frequency of the trained control policy is 20 Hz.

B. Simulation Setup

For simulation, we use IsaacGym [39], a highly parallelized rigid-body simulator, for training the teacher and student policies. We simulate the tactile observations by fetching the contact information from each fingertip. We use the local fingertip contact position (c_x, c_y, c_z) to calculate the contact pose angles, and the net contact force (F_x, F_y, F_z) to calculate the force magnitude $\|\mathbf{F}\|$. When required, the force magnitude is used to binarize the contact signal using a threshold similar to the real tactile sensor, $c_t = \{1 \text{ if } \|\mathbf{F}\| > 0.25 N; 0 \text{ otherwise}\}$. Since our tactile sensor has a soft tip, we made several modifications to make the tactile readings more realistic. First, we apply an exponential moving average on the net contact force readings to simulate the sensing delay due to elastic deformation. We also saturate and re-scale the

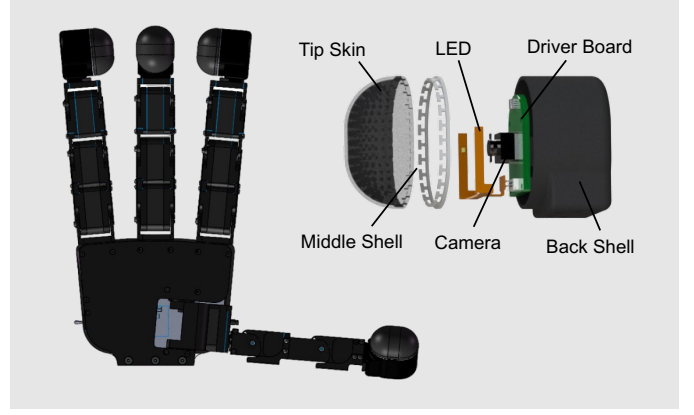


Fig. 2: CAD models of the fully-actuated (Allegro) robot hand and integrated tactile sensors. The vision-based tactile sensor has a rounded skin surface appropriate for dexterous in-hand manipulation, and a custom base housing the camera and lighting (based on redesigning the DigiTac/DIGIT base [33]). These tactile sensors are mounted on the fingertips with offsets of (thumb, index, middle, ring) = $(-45^\circ, -45^\circ, 0^\circ, 45^\circ)$ to maximize the contact sensing during in-hand object rotation.

contact force magnitudes experienced on each fingertip to the possible ranges experienced in reality to overcome any force-reading inaccuracies. In the real world, the contact pose ranges are naturally limited by the softness; therefore, we also apply similar saturation and re-scaling of the contact pose readings to minimize the sim-to-real gap. We run the simulation at 60 Hz and robot control at 20 Hz, which is the same as in reality.

IV. METHOD

In this paper, we investigate gravity invariant in-hand object rotation via stable precision grasping, a process for continuous object rotation in different hand directions without a supporting surface. We assume a stationary problem where the hand orientation is randomly initialized between episodes but remains fixed during the task. However, later we show that this policy can extend to a non-stationary scenario where the hand direction can continuously change during in-hand manipulation. We formulate the object-rotation problem as object reorientation to a target, where upon reaching a goal orientation, a new goal is generated by rotating the current goal about the desired rotation axis. This approach is particularly beneficial during early training phases, as a subgoal curriculum can provide more frequent rewards to avoid getting stuck at a local optima [4]. We also employ a two-stage learning process [31, 29]: the teacher is trained with privileged object and goal information using reinforcement learning, and the student is trained via supervised learning to imitate the teacher’s policy given a history of observations. An overview of our method can be found in Fig. 3.

A. Teacher Policy

We formulate the task as a finite horizon goal-conditioned Markov Decision Process (MDP) $\mathcal{M} = (\mathcal{S}, \mathcal{A}, \mathcal{R}, \mathcal{P}, \mathcal{G})$, defined by a continuous state $s \in \mathcal{S}$, a continuous action space $a \in \mathcal{A}$, a probabilistic state transition function $p(s_{t+1}|s_t, a_t) \in$

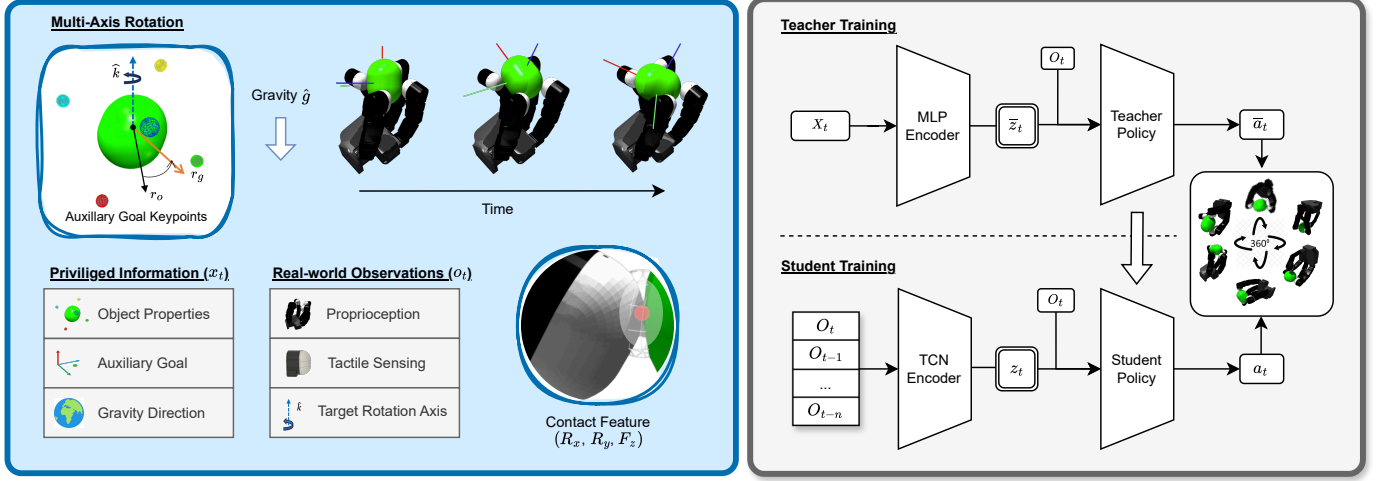


Fig. 3: Overview of approach for training the tactile policy in simulation and deploying in the real world. *Left:* The object rotation problem is formulated as an object reorientation to a goal and we use an auxiliary goal keypoint formulation to achieve object rotation about any chosen target axis. *Right:* We train a policy using a teacher-student policy distillation, the teacher is trained with RL and has access to privileged information, the student aims to imitate the teacher’s action given a history of tactile and proprioception observations. Privileged information and real-world observation are shown.

\mathcal{P} , a goal $g \in \mathcal{G}$ and a reward function $r \in \mathcal{R} : \mathcal{S} \times \mathcal{A} \times \mathcal{G} \rightarrow \mathbb{R}$. At each time step t , a learning agent selects an action a_t from the current policy $\pi(a_t|s_t, g)$ and receives a reward r . The aim is to obtain a policy π_θ^* parameterized by θ that maximizes the expected return over an episode τ and goals g given by:

$$\pi_\theta^* = \arg \max_{\pi} \mathbb{E}_{\tau \sim p_\pi(\tau), g \sim q(g)} \left[\sum_{t=0}^T \gamma^t r(s_t, a_t, g) \right], \quad (1)$$

where $\gamma \in [0, 1]$ is the discount factor, $p_\pi(\tau)$ is a distribution over episodes conditioned on π , and $q(g)$ is a distribution over the goal space \mathcal{G} with $g \in \mathcal{G}$.

We assume that the environment is fully observable. The state input is defined as $\langle O_t, X_t \rangle$ where O_t is the observation vector obtained from the real world and X_t is the privileged information available only in simulation. We train the teacher policy with input $\bar{a}_t = \pi_\theta(O_t, a_{t-1}, \bar{Z}_t)$, where the latent vector $\bar{Z}_t = \mu(X_t)$ is a low-dimensional encoding of the privileged information. We use an MLP encoder for $\mu(x)$ and an actor-critic architecture trained with PPO [52, 38].

1) Observation Space: The observation O_t contains the current and target joint position $q_t, \bar{q}_t \in \mathbb{R}^{16}$, previous action $a_{t-1} \in \mathbb{R}^{16}$, fingertip position $f_t^p \in \mathbb{R}^{12}$, fingertip orientation $f_t^r \in \mathbb{R}^{16}$, binary contact $c_t \in [0, 1]^4$, contact pose $P_t \in \mathbb{S}^4$, contact force magnitude $F_t \in \mathbb{R}^4$, and the desired rotation axis $\hat{k} \in \mathbb{S}^2$. In the real world, the fingertip position and orientation are calculated relative to the hand frame using the joint position and a forward kinematic solver. Fingertip binary contact, contact pose, and contact force magnitude are obtained from processing the tactile sensor images. The privileged information provided to the teacher policy in simulation includes object position, orientation, angular velocity, dimensions, gravity forces on the center of mass, and the current goal orientation.

2) Action Space: At each time step, the action output from the policy is $a_t := \Delta\theta \in \mathbb{R}^{16}$, which represents the

relative joint positions of the robot hand. To encourage smooth finger motion, we also apply an exponential moving average to compute the target joint positions. The target joint position is then defined as $\bar{q}_t = \bar{q}_{t-1} + \tilde{a}_t$, where $\tilde{a}_t = \eta a_t + (1 - \eta) a_{t-1}$. This target joint command is sent to a PD torque controller to move the fingers of the hand. We control the hand at 20 Hz and limit the relative joint angles per time step to $\Delta\theta \in [-0.026, 0.026]^{16}$ rad.

3) Grasp Initialization and Resets: The objective of the object rotation task is to rotate the object stably in a precision grasp about a desired rotation axis. Before training, we collect stable grasps by randomly sampling object poses and joint positions. A grasp is deemed stable if the object can remain in the hand for the entire episode with random perturbations applied. The saved grasps are then used to reset the environment for object rotation.

4) Auxiliary Goal: The rotation axis is defined relative to the hand axis (which is considered the global frame of reference). At reset, we randomly generate a target rotation axis and gravity direction which remain fixed throughout the episode. For training a unified policy for multi-axis rotations, a formulation of the reward function using angular velocity will lead to inefficient training and convergence difficulties. Therefore, to improve training performance, we design a subgoal curriculum and formulate the object-rotation problem as object reorientation, where goals are placed about the rotation axis. We generate the first target by rotating the starting object orientation by a rotation increment about the rotation axis. Once the goal has been reached, we then perform the same operation again by rotating the previous goal and this is repeated until the episode ends. The rotation increment is a regular interval. A stable rotation is achieved when the rotation axis vector relative to the object (local) remains close to the global rotation axis. To reduce unnecessary exploration, the episode resets if the local rotation vector deviates above a set

threshold or if the object falls out of the hand.

5) **Reward Design:** In the following formulation, we design a goal-based reward function to achieve continuous rotation while also avoiding inefficient hand motion, of the form

$$r = r_{\text{rotation}} + r_{\text{contact}} + r_{\text{stable}} + r_{\text{terminate}}, \quad (2)$$

where:

$$r_{\text{rotation}} = \lambda_{\text{kp}} r_{\text{kp}} + \lambda_{\text{rot}} r_{\text{rot}} + r_{\text{bonus}},$$

$$r_{\text{contact}} = \lambda_{\text{gc}} r_{\text{gc}} + \lambda_{\text{bc}} r_{\text{bc}},$$

$$r_{\text{stable}} = \lambda_{\omega} r_{\omega} + \lambda_{\text{pose}} r_{\text{pose}} + \lambda_{\text{work}} r_{\text{work}} + \lambda_{\text{torque}} r_{\text{torque}},$$

$$r_{\text{terminate}} = \lambda_{\text{penalty}} \{1 : \text{fall or axis} > 45^\circ; 0 : \text{otherwise}\}.$$

The different terms in this reward are explained below.

The first part of the reward r_{rotation} is the continual object rotation objective. We use a keypoint formulation to define target pose, as has been used previously for object reorientation tasks [3]. Keypoints are object geometry independent and offer a smooth reward function that provides a natural balance between the position and orientation information of the object 6D pose. We use a logistic kernel, $\mathcal{K}(x) = (e^{ax} + b + e^{-ax})^{-1}$, where a and b are kernel parameters. This gives the keypoint reward as $r_{\text{kp}} = \frac{1}{N} \sum_{i=1}^N \mathcal{K}(\|k_i^o - k_i^g\|)$, where k_i^o and k_i^g are object and goal keypoints. We also use the keypoint distance to define a goal update tolerance d when $\frac{1}{N} \sum_{i=1}^N \|k_i^o - k_i^g\| < d$.

The overall objective is to reach as many targets as possible during an episode. However, when a new target pose is generated, this can cause a sudden drop in the keypoint distance reward and so lead to situations where the object is rotated near the target but not reach it. To avoid this, we add a sparse bonus reward r_{bonus} when a goal is reached. To further encourage continuous rotation even in cases where the object has missed a goal, we also include a rotation reward defined by the change in object rotation about the target rotation axis $r_{\text{rot}} = \text{clip}(\Delta\Theta \cdot \hat{k}; -c, c)$. We clip this reward to offer smooth rotation. We found these reward combinations offered a smoother rotational reward function in different phases of the learning object rotation task.

Much like a human fingertip, the morphology of the tactile sensor used here (Section III) provides the most accurate tactile sensing information when the contact is normal to the fingertip. Therefore, to discourage the robot from leveraging other parts of the sensor, such as the tip edge or camera casing, we include a contact reward r_{contact} in the second term of the reward function, which rewards tip contacts and penalizes contacts with any other parts of the hand. In the third term of the reward function, we include a term to encourage stable rotations r_{stable} , which helps with generating policies that are more transferable to the real world, comprising: an object angular velocity penalty, r_{ω} ; a hand-pose penalty on the distance between the joint position from a canonical pose, r_{pose} ; a controller work-done penalty, r_{work} ; and a torque applied penalty r_{torque} . We found that this combination of contact and stability rewards generated natural-looking policies.

Finally, we include an early termination penalty $r_{\text{terminate}}$ if the object falls out of the grasp or if the local rotation axis deviates too far from the global rotation axis.

6) **Adaptive Curriculum:** The learning of precision-grasp in-hand rotation task can be separated into two main stages, where the agent must first learn to stably grasp the object in different hand orientations before learning to rotate it stably about the desired rotation axis. Whilst the r_{contact} and r_{stable} reward terms are beneficial for the final policy, these terms are not related to the object rotation task and can result in a local optima where the object will be stably grasped without being rotated. To alleviate this issue, we apply a reward curriculum coefficient $\lambda_{\text{rew}} \times (r_{\text{contact}} + r_{\text{stable}})$, which increases linearly with the average number of rotations achieved per episode. We also employ a gravity curriculum similar to [13], which increases the gravity with average rotation to improve the sample efficiency further. However, we found this second curriculum to be less critical for successful training.

B. Student Policy Training

The policy trained in section IV-A uses privileged information, such as object properties and auxiliary goal pose, which are not available in the real world. Similar to previous work [47, 48], we use policy distillation to train a student policy that takes proprioception and tactile history as input to imitate the teacher policy. The student policy has the same actor-critic architecture as the teacher policy $a_t = \pi_{\theta}(O_t, a_{t-1}, Z_t)$ and returns a Gaussian distribution with diagonal covariances $a_t \equiv \mathcal{N}(\mu_{\theta}, \Sigma_{\theta})$. The latent vector $Z_t = \phi(O_t, O_{t-1}, \dots, O_{t-n})$ is the predicted low dimensional encoding from a sequence of N proprioceptive and tactile observations. We use a temporal convolutional network (TCN) encoder for the latent vector function $\phi(x)$.

We randomly initialize the student encoder network and initialize the policy network with the weights from the teacher policy. We train both the encoder and policy network via supervised learning with the mean squared error (MSE) of the latent vector and negative log-likelihood loss (NLL) of the action,

$$\mathcal{L} = \text{MSE}(z_t, \bar{z}_t) + \text{NLL}(\mu_{\theta}, \Sigma_{\theta}, \bar{a}_t). \quad (3)$$

A central hypothesis of the policy distillation method is that the latent vector \bar{z} can be (partially) recovered from a sequence of proprioceptive and tactile observations. The teacher policy uses the privileged object and goal information to provide the target latent vector for the in-hand rotation problem. However, without explicit object or goal information, the student policy may not be able to achieve the same level of goal-reaching tolerance, which can lead to missing the goal and collecting out-of-distribution data. To alleviate this performance issue, we use a distance tolerance $d = 0.15$ during teacher training and a larger goal update tolerance of $d = 0.25$ during student training.

C. Tactile Feature Extraction

The dense tactile observations considered here are continuous readings of contact pose and contact force predicted from the tactile images. For bridging the sim-to-real gap, we adopt the sim-to-real framework from Ref. [61] and train an observation model to perform zero-shot sim-to-real policy

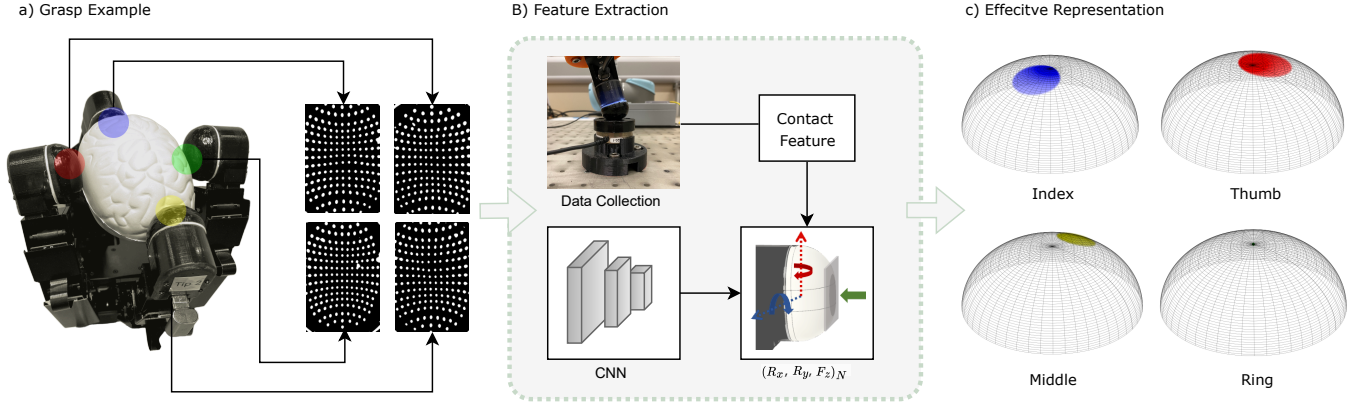


Fig. 4: A grasp example to demonstrate the tactile prediction pipeline. a) The tactile images on each fingertip are first preprocessed to provide grey-scale filtered images. b) The images are input to observation models for each tactile sensor to provide explicit features of the contact. These features are used as tactile observations for the RL policy. c) The effective tactile representation is visualized, showing the contact pose in spherical coordinates, and contact force as the size of the shaded area.

transfer. Given a real tactile image, we train a CNN model to extract the explicit features of contact. We assume the tactile features of this task are related to the geometry of the sensing surfaces, and so use spherical coordinates to simplify contact definitions with contact pose variables of polar angle R_x and azimuthal angle R_y relative to the fingertip origin. The predicted contact force variable is the total force magnitude of the contact. We also compute a binary contact signal using a Structured Similarity Index Measure (SSIM) threshold between the current and the reference tactile image and use this to mask contact pose and force predictions. An overview of the tactile prediction pipeline is shown in Fig. 4.

For data collection, we use a 6-DoF UR5 robot arm with our custom TacTip sensor attached to the end effector and a F/T sensor placed on the workspace platform. We collect data by moving the tactile sensor to randomly sampled poses over the surface of the flat stimulus mounted above the F/T sensor. For each interaction, we store tactile images with their corresponding pose and force labels. The target labels for this task are R_x and R_y of the end effector poses and (F_x, F_y, F_z) from the force readings of the F/T sensor. We select sample pose ranges of the end effector to determine effective contact pose ranges for sensing. For effective force ranges, we choose ranges in depth z , x -shear S_x and y -shear S_y of each contact interaction to obtain force readings up to 5 N. The magnitude of the predicted force vector is calculated to return the contact force observation.

V. SIMULATION EXPERIMENT

A. Training Performance

1) *Experiment Setup:* We first investigate the importance of our reward design and adaptive curriculum for learning the in-hand object rotation task. We compare our teacher training performance against the following baselines:

w/o auxiliary goal - We design an alternative formulation of the task by replacing the goal-driven terms in the reward function with angular velocity instead, to study if the task

can be learned without using auxiliary goals. We remove goal orientation from privileged information and also add a rotation axis penalty to encourage stable rotation.

w/o curriculum - We also train a teacher policy without the adaptive reward curriculum to study if the agent can learn the task without guidance.

2) *Results:* We compare the performance of our formulation with the baselines for both the single-axis and multi-axis object rotation. The learning curves for average rotation and successive goals reached are shown in Fig. 5. We observe that with an angular velocity formulation, the agent can learn the task in the single-axis setting, but with much lower accuracy. We obtain near-zero successive goals reached despite having a rotation axis penalty. In the multi-axis setting, the training was unsuccessful and the agent was unable to maintain stable rotation. The axis of rotation would often deviate to other undesirable axes, leading to inefficient learning. We were unable to find a reward using angular velocity that would solve both tasks.

The results also showed that the agent failed to learn without the adaptive reward curriculum. The resulting policy showed the agent getting stuck at a local optima where it keeps the object stable without dropping it. We suspect this is due to the initialization, where the task begins in an unstable grasping state and small random actions can lead to irrecoverable states, triggering the termination condition of this problem. This suggests that this is a difficult exploration problem and without the guidance of an adaptive curriculum, the agent cannot escape this local optima.

B. Tactile Sensing

1) *Experiment Setup:* We study the importance of rich tactile sensing for gravity-invariant multi-axis in-hand object rotation by training policies with different tactile observations in the policy input O_t . We use fundamental geometric shapes provided by Isaac Gym (capsule and box of varying size and mass) for training and we test the performance on two

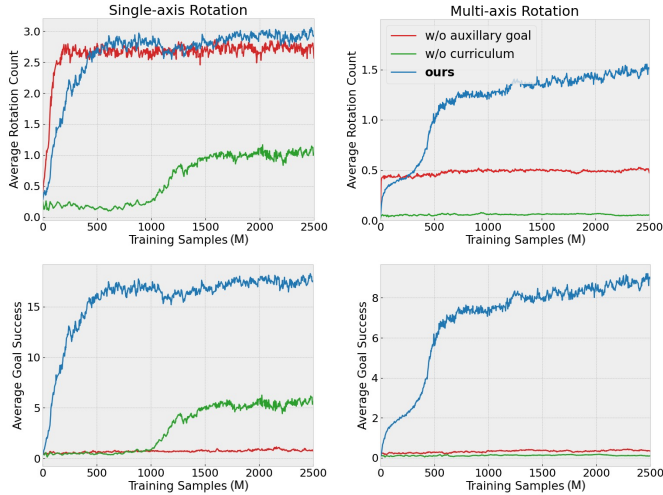


Fig. 5: Reinforcement learning curves for different training strategies. *Left:* Single-axis training where the target rotation axis remains fixed in the z-axis direction. *Right:* Multiple-axis training where the target rotation axis is randomized at the beginning of the episode. We report on the average rotation count (*top*) and the number of successive goals reached (*bottom*) over training. In both cases, the policy using our formulation trained more successfully, which became more pronounced in the multi-axis setting.

object sets 1) a heavy object set: training objects with out-of-distribution mass, 2) an unseen object set: a selection of unseen objects with uniform and nonuniform shapes (Fig. 6). It is worth noting that our in-hand rotation task differs from the one presented in [47, 48] where the object was resting on omnidirectional fingertips during manipulation. In our case, the fingertips are facing normal to the object. This means that we do not rely on specific direction of gravitational force to provide stable grasping support, the grasping and rotation motion comes entirely from contact between the fingers and the object. This makes the desired interaction more robust to external forces, but it also makes achieving stable gaiting more challenging, as any small mistake in the system can easily result in slippage and failure of the task.

We compare our **dense touch** policy which is trained with a continuous tactile signal of contact pose and contact force with the following baselines:

Proprio - a proprioception policy without any tactile information in the observation O_t .

Proprio w/o Gravity - for studying the effects of varying gravity, we also train a proprioception policy by fixing the hand the ‘palm up’ configuration to see whether the task can be solved without considering gravity invariance.

Binary Touch - a policy with added binary tactile observation. This is the lowest dimension for tactile sensing as it only provides an on/off contact signal for each fingertip.

Discrete Touch - a policy with discretized contact location, which was introduced in [48]. This is another form of low-dimensional tactile representation that discretizes the 3D contact location into N segments projected onto a 2D frame. We use the same number of segments $N = 8$ for our experiment.

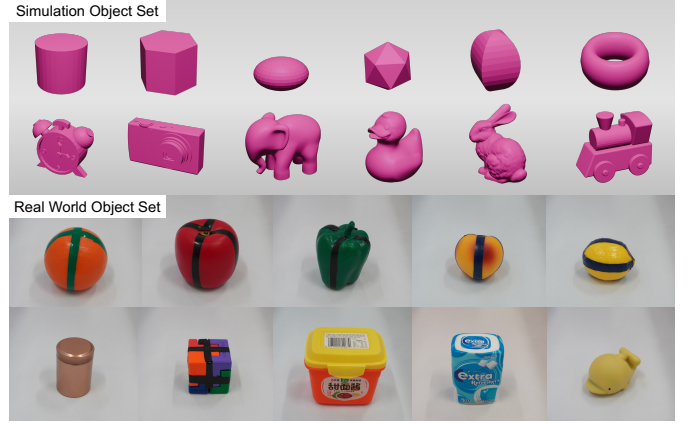


Fig. 6: *Top:* Simulation object set containing uniform objects (*row 1*) and nonuniform objects obtained from the ContactDB dataset [10] (*row 2*). *Bottom:* real-world object set containing objects of varying shape, size, and mass. Tape is wrapped on round objects so that the rotation is visible.

TABLE I: Simulation performance of different tactile policies on test object sets. We report on average rotation achieved per episode (Rot) and average episode length (EpLen).

Observation	Heavy Object Set		Unseen Object Set	
	Rot	EpLen(s)	Rot	EpLen(s)
Proprio w/o Gravity	0.55	11.8	0.55	19.1
Proprio	1.34	21.5	0.82	25.1
Binary Touch	1.90	20.8	1.57	25.3
Discrete Touch	1.95	22.2	1.67	26.6
Dense Touch w/o Pose	2.05	22.0	1.60	25.5
Dense Touch w/o Force	2.05	21.9	1.73	26.7
Dense Touch (Ours)	2.18	22.8	1.77	27.2

We also train two additional policies with dense tactile sensing for ablation purposes, **Dense Touch w/o Pose** is a policy containing only the contact force and **Dense Touch w/o Force** containing only the contact pose, to study the importance of individual contact features.

2) *Results:* We evaluate the performance based on average rotation achieved per episode (Rot) and average episode length (EpLen). The results are shown in Table I. The proprioception policy trained with a fixed hand orientation performed poorly when testing in arbitrary hand orientations. Despite the object being in grasp during manipulation, the results suggest that gravity invariance is still important for this task and different hand orientations require different controls for stable object rotation. Contrary to the findings in [48], we do find binary contact to be beneficial over proprioception alone despite including joint history. We suspect this is due to including binary contact information during the reinforcement learning stage, which helps with learning a better teacher policy. This is aligned with prior work in [27].

We observed that performance improved with more detailed tactile sensing. The dense touch policy, which provided continuous information about contact pose and force, outperformed

other methods that used simpler, less detailed touch for both test object sets. We found that discretizing the contact location led to a drop in performance, suggesting that this type of representation is not as well suited to the morphology of our sensor. The discretization was designed at the center of the fingertip where most contact occurs and this can lead to noisy tactile readings that are less informative of the contact state. Our ablation studies showed that omitting contact pose led to a drop in performance for both test object sets, suggesting that contact pose is an important feature for in-hand object rotation. We also see in the Dense Touch w/o Force policy, that contact pose alone was unable to match the performance of dense touch, especially for heavy objects, demonstrating the importance of the force features when handling objects with varying weights. Excluding either feature of tactile sensing in the policy resulted in suboptimal performance.

VI. REAL-WORLD EXPERIMENT

We validate our methods in the real world by testing in different hand orientations and rotation axes using the setup described in Sec. III. The key objective is to study if rich tactile sensing can be successfully transferred to the real world using our proposed dense tactile representation and trained observation model; we also examine if tactile sensing provides any additional benefits when coping with the effect of various gravity directions and the sim-to-real gap.

A. Experiment Setup

We first experiment with object rotation about the z -axis on six principal directions of the hand, palm up, palm down, base up, base down, thumb up, and thumb down (see Fig. 1) to investigate the effects of different gravity directions on the manipulation performance. We then fix the hand in the palm down direction, a common hand direction for everyday manipulation, and experiment with object rotation across the three principal x , y , and z -axes. We test on 10 real-world objects which consist of unseen objects of different shapes and sizes (see Fig. 6). We made our best attempt at system identification and then kept the control gains constant throughout training and testing in simulation and the real world. More information regarding system identification and test objects can be found in the supplementary material.

To validate the sim-to-real transfer, we compare our dense touch policy with the proprioception and binary touch policy in the real-world experiment. The binary touch policy uses SSIM to infer contact signals and does not require an observation model for sim-to-real transfer. We found that the proprioception policy without gravity invariance failed to transfer to the real world for unseen hand directions. We run the experiment for 600 steps which equates to 30 seconds and use the following metrics for evaluation:

Rotation Count (Rot) - the total number of rotations achieved per episode. We attach reference markers on the object (visible as the tape in Fig 6) and manually count the number of rotations achieved.

Time to Terminate (TTT) - We measure the time taken before

the object gets stuck, falls out of the hand, or if the local rotation axis has deviated by more than 90° .

B. Results and Discussion

The results for various hand orientations and rotation axes are detailed in Tables II and III. In both cases, the policy trained with dense touch performed the best in the real world, demonstrating a successful transfer of the tactile policy. The proprioception and binary touch policy were less effective at maintaining stable rotation, often resulting in loss of contact or getting stuck. We found that generally, the performance was better for the palm up and palm down hand directions, followed by base up and base down, with the thumb up and thumb down resulting in the worst performance. We suspect this is due to the larger sim-to-real gap of the Allegro hand when the fingers are positioned horizontally during manipulation. Here the gravity loading of the fingers acts directly against joint actuation, significantly weakening the capabilities of the hand. However, despite the noisy system, a policy provided with detailed tactile information consistently demonstrated stable object rotation. Sample frames of object rotation can be found in Fig. 8. When comparing different rotation axes, the z -axis was the easiest to achieve, followed by the x - and y -axes. We noticed that binary touch had similar results to proprioception when rotating about the z -axis, but did provide benefits around the x - and y -rotation axes. These axes require two fingers to hold the object steady (middle/thumb or index/pinky) while the remaining two fingers provide a stable rotating motion. This rotation is much harder to achieve and the policy struggled to perform well with proprioception alone.

1) **Sensor Response:** A more complete analysis of the tactile sensor signals during a rollout of a policy is shown in Fig. 7 for the palm-down hand orientation rotating around the z -axis. The two key motions for stable object rotation can be seen in the two contact pose angle trajectories, R_x and R_y . Evidently, R_y provides the main rotation component, where the angle periodically increases before breaking contact, representing the motion of the object rolling along the fingertip (blue-shaded region). Meanwhile, R_x provides the stability component, detecting when the object is slowly slipping out of stable grasp. When the angle for the R_x component becomes too high, an adaptive behavior occurs (grey-shaded region) where the fingers extend along the object to reduce this angle and avoid the object slipping out of grasp. The contact force component aims to maintain a constant force on the grasp during the rotation motion. Altogether, these components of tactile sensing work together with the finger gaiting motion to ensure stable rotation without slipping, highlighting the benefits of information-rich tactile sensing.

2) **Inferring Object Properties:** In our experiment, we found the dense touch policy was most effective for round or ellipsoidal objects. We attributed this behavior was due to the ability to estimate object position using the contact pose of each finger, allowing the policy to adapt and move to a stable center for grasping manipulation. For objects that are more boxed-shaped or of larger aspect ratios, some grasping points

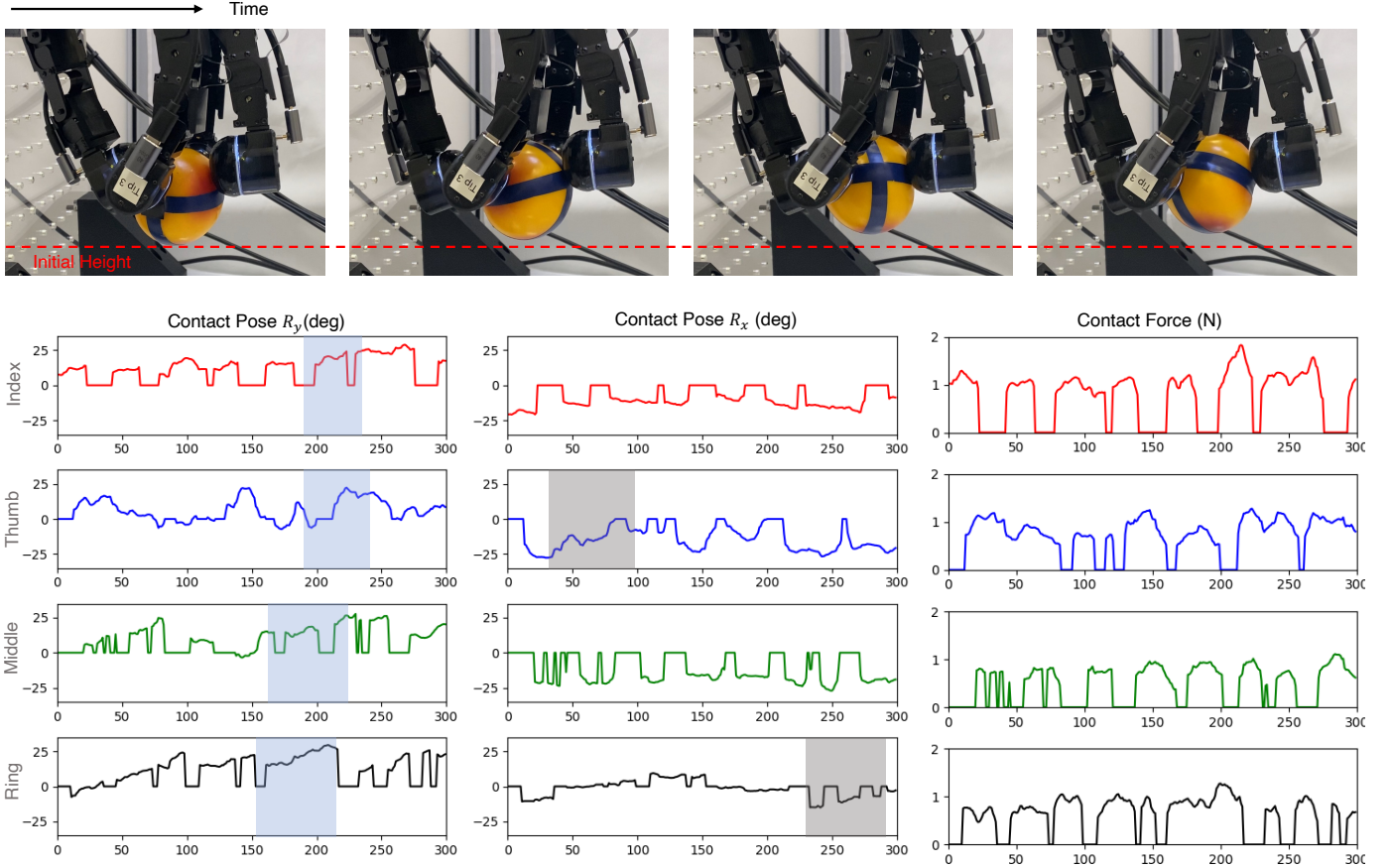


Fig. 7: Example in-hand rotation performance for rotating about the z -axis with the hand oriented to palm down. An SSIM threshold of 0.6 is applied for contact detection, equating to $\approx 0.25N$. Contacts that exert a force below this threshold are neglected. The contact pose components (R_x, R_y) and contact force are plotted for each of the four fingers, gated to zero when there is no contact detection. The blue-shaded region represents the rotation component of contact, where the object rolls along the fingertip in the R_y direction. The grey-shaded region represents the stability component where the fingers extend under edge contact to maintain a stable grasp. The force component remains steady under contact throughout the gaining motion.

TABLE II: Real-world performance of policies trained on different observations for rotating about the z -axis in different hand directions. The experiment was repeated 3 times for each object and averaged over the test object set. We compare using the metric rotation count (rot) and time to terminate (TTT) per episode.

Observation	Palm Up		Palm Down		Base Up		Base Down		Thumb Up		Thumb Down	
	Rot	TTT(s)	Rot	TTT(s)	Rot	TTT(s)	Rot	TTT(s)	Rot	TTT(s)	Rot	TTT(s)
Proprio	1.47	27.6	1.05	25.3	0.84	26.8	0.87	23.5	0.78	20.3	0.51	9.75
Binary Touch	1.32	25.5	0.89	23.8	0.86	25.3	0.77	22.0	0.83	22.6	0.47	12.3
Dense Touch (Ours)	1.57	30.0	1.33	28.2	1.32	29.8	1.17	29.4	1.08	27.9	0.91	29.2

can produce similar tactile information but represent different states of the system. Finding a stable grasping center with touch in this case becomes much more challenging. We believe that a richer tactile representation, such as tactile images, could further improve the performance by providing additional contact features such as surfaces or edges. We also limit the contact force to just 1D force magnitude to minimize the sim-to-real gap. Extending this to 3D contact forces could help infer additional properties, such as mass or friction, which may be useful when adapting to heavier objects or sticky contacts.

3) Applications: Whilst we performed in-hand rotation in a static setting by fixing the hand direction during the experiment, we can show that the same system and policy is capable of adapting to a non-stationary hand when moving the end effector of the robot arm, suggesting strong robustness to changes in forces caused by the movement of the hand, due to either linear or angular motion. The ability to rotate objects about any axis while the hand is in motion opens up broader possibilities. A combined robot arm-hand system could then efficiently execute general pick-and-place tasks for objects

TABLE III: Real-world performance of policies trained on different observations for rotating about different rotation axis in the palm down configuration. The experiment was repeated 3 times for each object and averaged over the test object set. We show the metric for rotation count and time to terminate (TTT) per episode.

Observation	x-axis		y-axis		z-axis	
	Rot	TTT(s)	Rot	TTT(s)	Rot	TTT(s)
Proprio	0.35	16.6	0.17	8.33	1.05	25.3
Binary Touch	0.87	26.5	0.25	15.9	0.89	23.8
Dense Touch	1.33	28.6	0.79	27.8	1.33	28.2

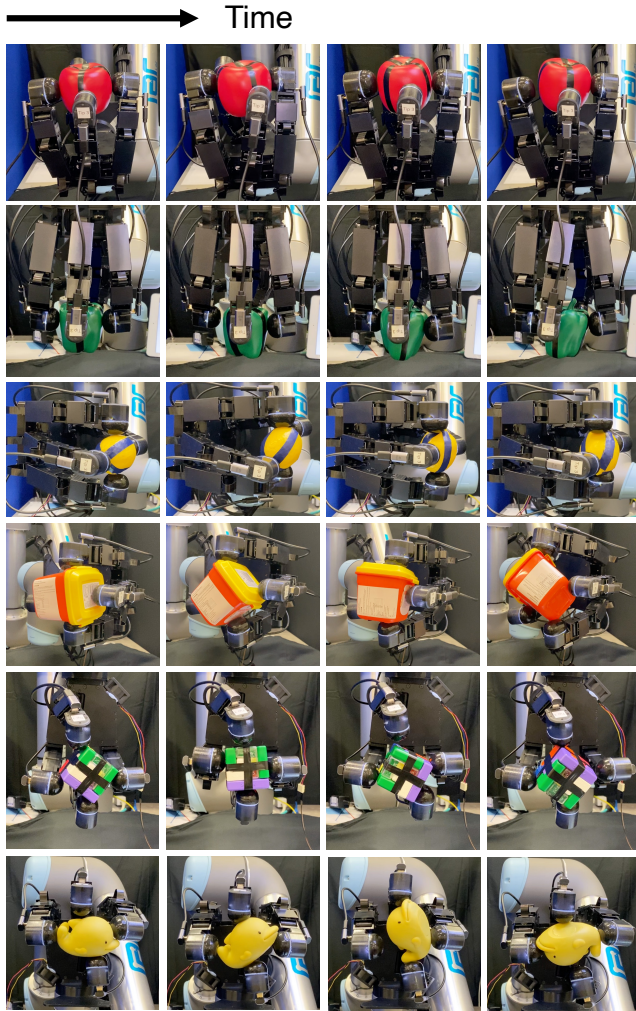


Fig. 8: Examples of in-hand rotation for the six distinct objects under distinct hand orientations with respect to gravity.

in any three-dimensional position and orientation within the workspace, further enhancing the value of such a system. A demonstration of the in-hand rotation capability while moving the orientation of the hand with respect to gravity can be found in the last section of the supporting video.

VII. CONCLUSION

In this paper, we presented AnyRotate, a system to achieve multi-axis gravity-invariant object rotation with dense featured

sim-to-real touch. We presented an RL formulation with an auxiliary subgoal curriculum and a two-stage training strategy to successfully address the challenges of learning this difficult exploration problem. We proposed a dense tactile representation that could be used within a highly parallelized rigid-body simulator to enhance sensory feedback. Our ablation studies and analyses illustrated the advantages of various features of tactile sensing for handling objects with varying properties. We also introduced an approach for sim-to-real transfer of the dense tactile observations. We conducted extensive experiments in the real world over different hand orientations and rotation axes for a diverse object set to evaluate the robustness of our methods. The results demonstrated the role of rich tactile information in improving in-hand dexterity that overcomes the variability inherent in real world settings.

While our investigation has focused on a specific case of in-hand manipulation using tactile sensing, we expect that the opportunities extend far beyond our demonstrations. The capability to manipulate objects effortlessly in free space with a sense of touch mirrors an intuitive skill of human dexterity and stands as a significant goal in robotics. We hope that our research not only reaffirms the value of tactile sensing within the robotics community but also spurs continued efforts to reach a level of robot hand dexterity comparable to that of the human hand.

REFERENCES

- [1] Alexander C. Abad and Anuradha Ranasinghe. Visuotactile sensors with emphasis on gelsight sensor: A review. *IEEE Sensors Journal*, 20(14):7628–7638, July 2020.
- [2] Ilge Akkaya, Marcin Andrychowicz, Maciek Chociej, Mateusz Litwin, Bob McGrew, Arthur Petron, Alex Paino, Matthias Plappert, Glenn Powell, Raphael Ribas, et al. Solving rubik’s cube with a robot hand. *arXiv preprint arXiv:1910.07113*, 2019.
- [3] Arthur Allshire, Mayank Mittal, Varun Lodaya, Viktor Makoviychuk, Denys Makoviichuk, Felix Widmaier, Manuel Wüthrich, Stefan Bauer, Ankur Handa, and Animesh Garg. Transferring dexterous manipulation from gpu simulation to a remote real-world trifinger. In *2022 IEEE/RSJ International Conference on Intelligent Robots and Systems (IROS)*, pages 11802–11809. IEEE, 2022.
- [4] Marcin Andrychowicz, Filip Wolski, Alex Ray, Jonas Schneider, Rachel Fong, Peter Welinder, Bob McGrew, Josh Tobin, OpenAI Pieter Abbeel, and Wojciech Zaremba. Hindsight experience replay. *Advances in neural information processing systems*, 30, 2017.
- [5] OpenAI: Marcin Andrychowicz, Bowen Baker, Maciek Chociej, Rafal Jozefowicz, Bob McGrew, Jakub Pachocki, Arthur Petron, Matthias Plappert, Glenn Powell, Alex Ray, et al. Learning dexterous in-hand manipulation. *The International Journal of Robotics Research*, 39(1):3–20, 2020.
- [6] Yunfei Bai and C Karen Liu. Dexterous manipulation using both palm and fingers. In *2014 IEEE International*

- Conference on Robotics and Automation (ICRA)*, pages 1560–1565. IEEE, 2014.
- [7] Antonio Bicchi. Hands for dexterous manipulation and robust grasping: A difficult road toward simplicity. *IEEE Transactions on robotics and automation*, 16(6):652–662, 2000.
 - [8] Antonio Bicchi and Raffaele Sorrentino. Dexterous manipulation through rolling. In *Proceedings of 1995 IEEE International Conference on Robotics and Automation*, volume 1, pages 452–457. IEEE, 1995.
 - [9] Gary Bradski. The OpenCV Library. *Dr. Dobb’s Journal of Software Tools*, 2000.
 - [10] Samarth Brahmabhatt, Cusuh Ham, Charles C Kemp, and James Hays. Contactdb: Analyzing and predicting grasp contact via thermal imaging. In *Proceedings of the IEEE/CVF conference on computer vision and pattern recognition*, pages 8709–8719, 2019.
 - [11] Tao Chen, Megha Tippur, Siyang Wu, Vikash Kumar, Edward Adelson, and Pulkit Agrawal. Visual dexterity: In-hand dexterous manipulation from depth. *arXiv preprint arXiv:2211.11744*, 2022.
 - [12] Tao Chen, Jie Xu, and Pulkit Agrawal. A system for general in-hand object re-orientation. In *Conference on Robot Learning*, pages 297–307. PMLR, 2022.
 - [13] Tao Chen, Megha Tippur, Siyang Wu, Vikash Kumar, Edward Adelson, and Pulkit Agrawal. Visual dexterity: In-hand reorientation of novel and complex object shapes. *Science Robotics*, 8(84):eabc9244, 2023.
 - [14] Weihang Chen, Yuan Xu, Zhenyang Chen, Peiyu Zeng, Renjun Dang, Rui Chen, and Jing Xu. Bidirectional sim-to-real transfer for gelsight tactile sensors with cyclegan. *IEEE Robotics and Automation Letters*, 7(3):6187–6194, 2022.
 - [15] Zixi Chen, Shixin Zhang, Shan Luo, Fuchun Sun, and Bin Fang. Tacchi: A pluggable and low computational cost elastomer deformation simulator for optical tactile sensors. *IEEE Robotics and Automation Letters*, 8(3):1239–1246, 2023. doi: 10.1109/LRA.2023.3237042.
 - [16] Alex Church, John Lloyd, Raia Hadsell, and Nathan Lepora. Tactile Sim-to-Real Policy Transfer via Real-to-Sim Image Translation. In *Proceedings of the 5th Conference on Robot Learning*, pages 1–9. PMLR, October 2021.
 - [17] Paulo Paoletti Daniel F. Gomes and Shan Luo. Generation of gelsight tactile images for sim2real learning. *IEEE Robotics and Automation Letters*, 6(2):4177–4184, April 2021.
 - [18] Yongxiang Fan, Wei Gao, Wenjie Chen, and Masayoshi Tomizuka. Real-time finger gaits planning for dexterous manipulation. *IFAC-PapersOnLine*, 50(1):12765–12772, 2017.
 - [19] Ronald Fearing. Implementing a force strategy for object re-orientation. In *Proceedings. 1986 IEEE International Conference on Robotics and Automation*, volume 3, pages 96–102. IEEE, 1986.
 - [20] Xiao Gao, Kunpeng Yao, Farshad Khadivar, and Aude Billard. Real-time motion planning for in-hand manipulation with a multi-fingered hand. *arXiv preprint arXiv:2309.06955*, 2023.
 - [21] Li Han and Jeffrey C Trinkle. Dextrous manipulation by rolling and finger gaiting. In *Proceedings. 1998 IEEE International Conference on Robotics and Automation (Cat. No. 98CH36146)*, volume 1, pages 730–735. IEEE, 1998.
 - [22] Li Han, Yi-Sheng Guan, ZX Li, Q Shi, and Jeffrey C Trinkle. Dextrous manipulation with rolling contacts. In *Proceedings of International Conference on Robotics and Automation*, volume 2, pages 992–997. IEEE, 1997.
 - [23] Ankur Handa, Arthur Allshire, Viktor Makoviychuk, Aleksei Petrenko, Ritvik Singh, Jingzhou Liu, Denys Makoviichuk, Karl Van Wyk, Alexander Zhurkevich, Balakumar Sundaralingam, et al. Dextreme: Transfer of agile in-hand manipulation from simulation to reality. In *2023 IEEE International Conference on Robotics and Automation (ICRA)*, pages 5977–5984. IEEE, 2023.
 - [24] Binghao Huang, Yuanpei Chen, Tianyu Wang, Yuzhe Qin, Yaodong Yang, Nikolay Atanasov, and Xiaolong Wang. Dynamic handover: Throw and catch with bi-manual hands. *arXiv preprint arXiv:2309.05655*, 2023.
 - [25] Tudor Jianu, Daniel Fernandes Gomes, and Shan Luo. Reducing tactile sim2real domain gaps via deep texture generation networks. *arXiv preprint arXiv:2112.01807*, 2021.
 - [26] Farshad Khadivar and Aude Billard. Adaptive fingers coordination for robust grasp and in-hand manipulation under disturbances and unknown dynamics. *IEEE Transactions on Robotics*, 2023.
 - [27] Gagan Khandate, Maximilian Haas-Heger, and Matei Ciocarlie. On the feasibility of learning finger-gaiting in-hand manipulation with intrinsic sensing. In *2022 International Conference on Robotics and Automation (ICRA)*, pages 2752–2758. IEEE, 2022.
 - [28] Gagan Khandate, Siqi Shang, Eric T Chang, Tristan Luca Saidi, Johnson Adams, and Matei Ciocarlie. Sampling-based exploration for reinforcement learning of dexterous manipulation. *arXiv preprint arXiv:2303.03486*, 2023.
 - [29] Ashish Kumar, Zipeng Fu, Deepak Pathak, and Jitendra Malik. Rma: Rapid motor adaptation for legged robots. *arXiv preprint arXiv:2107.04034*, 2021.
 - [30] Mike Lambeta, Po-Wei Chou, Stephen Tian, Brian Yang, Benjamin Maloon, Victoria Rose Most, Dave Stroud, Raymond Santos, Ahmad Byagowi, Gregg Kammerer, et al. Digit: A novel design for a low-cost compact high-resolution tactile sensor with application to in-hand manipulation. *IEEE Robotics and Automation Letters*, 5(3):3838–3845, 2020.
 - [31] Joonho Lee, Jemin Hwangbo, Lorenz Wellhausen, Vladlen Koltun, and Marco Hutter. Learning quadrupedal locomotion over challenging terrain. *Science robotics*, 5(47):eabc5986, 2020.
 - [32] Nathan F Lepora. Soft Biomimetic Optical Tactile Sensing With the TacTip: A Review. *IEEE Sensors Journal*, 21(19):21131–21143, October 2021. ISSN 1530-

- 437X, 1558-1748, 2379-9153. doi: 10.1109/JSEN.2021.3100645.
- [33] Nathan F Lepora, Yijiong Lin, Ben Money-Coomes, and John Lloyd. Digitac: A digit-tactip hybrid tactile sensor for comparing low-cost high-resolution robot touch. *IEEE Robotics and Automation Letters*, 7(4):9382–9388, 2022.
 - [34] Susanna Leveroni and Kenneth Salisbury. Reorienting objects with a robot hand using grasp gaits. In *Robotics Research: The Seventh International Symposium*, pages 39–51. Springer, 1996.
 - [35] Yijiong Lin, John Lloyd, Alex Church, and Nathan Lepora. Tactile gym 2.0: Sim-to-real deep reinforcement learning for comparing low-cost high-resolution robot touch. volume 7 of *Proceedings of Machine Learning Research*, pages 10754–10761. IEEE, August 2022. doi: 10.1109/LRA.2022.3195195. URL <https://ieeexplore.ieee.org/abstract/document/9847020>.
 - [36] Yijiong Lin, Alex Church, Max Yang, Haoran Li, John Lloyd, Dandan Zhang, and Nathan F Lepora. Bi-touch: Bimanual tactile manipulation with sim-to-real deep reinforcement learning. *IEEE Robotics and Automation Letters*, 2023.
 - [37] Quan Khanh Luu, Nhan Huu Nguyen, et al. Simulation, learning, and application of vision-based tactile sensing at large scale. *IEEE Transactions on Robotics*, 2023.
 - [38] Denys Makoviichuk and Viktor Makovychuk. rl-games: A high-performance framework for reinforcement learning. https://github.com/Denys88/rl_games, May 2021.
 - [39] Viktor Makovychuk, Lukasz Wawrzyniak, Yunrong Guo, Michelle Lu, Kier Storey, Miles Macklin, David Hoeller, Nikita Rudin, Arthur Allshire, Ankur Handa, et al. Isaac gym: High performance gpu-based physics simulation for robot learning. *arXiv preprint arXiv:2108.10470*, 2021.
 - [40] Andrew S Morgan, Kaiyu Hang, Bowen Wen, Kostas Bekris, and Aaron M Dollar. Complex in-hand manipulation via compliance-enabled finger gaiting and multi-modal planning. *IEEE Robotics and Automation Letters*, 7(2):4821–4828, 2022.
 - [41] Anusha Nagabandi, Kurt Konolige, Sergey Levine, and Vikash Kumar. Deep dynamics models for learning dexterous manipulation. In *Conference on Robot Learning*, pages 1101–1112. PMLR, 2020.
 - [42] Yashraj Narang, Balakumar Sundaralingam, Miles Macklin, Arsalan Mousavian, and Dieter Fox. Sim-to-real for robotic tactile sensing via physics-based simulation and learned latent projections. *arXiv preprint arXiv:2103.16747*, 2021.
 - [43] Allison M Okamura, Niels Smaby, and Mark R Cutkosky. An overview of dexterous manipulation. In *Proceedings 2000 ICRA. Millennium Conference. IEEE International Conference on Robotics and Automation. Symposia Proceedings (Cat. No. 00CH37065)*, volume 1, pages 255–262. IEEE, 2000.
 - [44] Tao Pang, HJ Terry Suh, Lujie Yang, and Russ Tedrake. Global planning for contact-rich manipulation via local smoothing of quasi-dynamic contact models. *IEEE Transactions on Robotics*, 2023.
 - [45] Johannes Pitz, Lennart Röstel, Leon Sievers, and Berthold Bäuml. Dextrous tactile in-hand manipulation using a modular reinforcement learning architecture. *arXiv preprint arXiv:2303.04705*, 2023.
 - [46] Robert Platt, Andrew H Fagg, and Roderic A Grupen. Manipulation gaits: Sequences of grasp control tasks. In *IEEE International Conference on Robotics and Automation, 2004. Proceedings. ICRA'04. 2004*, volume 1, pages 801–806. IEEE, 2004.
 - [47] Haozhi Qi, Ashish Kumar, Roberto Calandra, Yi Ma, and Jitendra Malik. In-hand object rotation via rapid motor adaptation. In *Conference on Robot Learning*, pages 1722–1732. PMLR, 2023.
 - [48] Haozhi Qi, Brent Yi, Sudharshan Suresh, Mike Lambeta, Yi Ma, Roberto Calandra, and Jitendra Malik. General in-hand object rotation with vision and touch. In *Conference on Robot Learning*, pages 2549–2564. PMLR, 2023.
 - [49] Lennart Röstel, Johannes Pitz, Leon Sievers, and Berthold Bäuml. Estimator-coupled reinforcement learning for robust purely tactile in-hand manipulation. In *2023 IEEE-RAS 22nd International Conference on Humanoid Robots (Humanoids)*, pages 1–8. IEEE, 2023.
 - [50] Daniela Rus. In-hand dexterous manipulation of piecewise-smooth 3-d objects. *The International Journal of Robotics Research*, 18(4):355–381, 1999.
 - [51] Jean-Philippe Saut, Anis Sahbani, Sahar El-Khoury, and Véronique Perdereau. Dexterous manipulation planning using probabilistic roadmaps in continuous grasp subspaces. In *2007 IEEE/RSJ International Conference on Intelligent Robots and Systems*, pages 2907–2912. IEEE, 2007.
 - [52] John Schulman, Filip Wolski, Prafulla Dhariwal, Alec Radford, and Oleg Klimov. Proximal policy optimization algorithms. *arXiv preprint arXiv:1707.06347*, 2017.
 - [53] Jian Shi, J Zachary Woodruff, Paul B Umbanhowar, and Kevin M Lynch. Dynamic in-hand sliding manipulation. *IEEE Transactions on Robotics*, 33(4):778–795, 2017.
 - [54] Zilin Si and Wenzhen Yuan. Taxim: An example-based simulation model for gelsight tactile sensors. *IEEE Robotics and Automation Letters*, pages 2361–2368, 2022.
 - [55] Leon Sievers, Johannes Pitz, and Berthold Bäuml. Learning purely tactile in-hand manipulation with a torque-controlled hand. In *2022 International Conference on Robotics and Automation (ICRA)*, pages 2745–2751. IEEE, 2022.
 - [56] Balakumar Sundaralingam and Tucker Hermans. Geometric in-hand regrasp planning: Alternating optimization of finger gaits and in-grasp manipulation. In *2018 IEEE International Conference on Robotics and Automation (ICRA)*, pages 231–238. IEEE, 2018.
 - [57] Clark B Teeple, Buse Aktaş, Michelle C Yuen, Grace R Kim, Robert D Howe, and Robert J Wood. Controlling

palm-object interactions via friction for enhanced in-hand manipulation. *IEEE Robotics and Automation Letters*, 7(2):2258–2265, 2022.

- [58] Shaoxiong Wang, Mike Lambeta, Po-Wei Chou, and Roberto Calandra. Tacto: A fast, flexible, and open-source simulator for high-resolution vision-based tactile sensors. *IEEE Robotics and Automation Letters*, 7(2): 3930–3937, 2022.
- [59] Benjamin Ward-Cherrier, Nicholas Pestell, Luke Cramphorn, Benjamin Winstone, Maria Elena Giannaccini, Jonathan Rossiter, and Nathan F Lepora. The tac-tip family: Soft optical tactile sensors with 3d-printed biomimetic morphologies. *Soft robotics*, 5(2):216–227, 2018.
- [60] Jie Xu, Sangwoon Kim, Tao Chen, Alberto Rodriguez Garcia, Pulkit Agrawal, Wojciech Matusik, and Shinjiro Sueda. Efficient tactile simulation with differentiability for robotic manipulation. In *Proceedings of The 6th Conference on Robot Learning*, volume 205 of *Proceedings of Machine Learning Research*, pages 1488–1498. PMLR, 14–18 Dec 2023. URL <https://proceedings.mlr.press/v205/xu23b.html>.
- [61] Max Yang, Yijiong Lin, Alex Church, John Lloyd, Dandan Zhang, David AW Barton, and Nathan F Lepora. Sim-to-real model-based and model-free deep reinforcement learning for tactile pushing. *IEEE Robotics and Automation Letters*, 2023.
- [62] Zhao-Heng Yin, Binghao Huang, Yuzhe Qin, Qifeng Chen, and Xiaolong Wang. Rotating without seeing: Towards in-hand dexterity through touch. *arXiv preprint arXiv:2303.10880*, 2023.
- [63] Wenzhen Yuan, Siyuan Dong, and Edward H. Adelson. GelSight: High-Resolution Robot Tactile Sensors for Estimating Geometry and Force. *Sensors*, 17(12):2762, December 2017. doi: 10.3390/s17122762.

APPENDIX

A. Observations

We present the full list of observations used for the agent in table IV and are available both in simulation and the real world. The proprioception and tactile dimensions are in multiples of four, representing four fingers.

TABLE IV: Full list of observations (O_t) available in simulation and the real world used for teacher and student policy.

Name	Symbol	Dimensions
Proprioception		
Joint Position	q	16
Fingertip Position	f^p	12
Fingertip Orientation	f^o	16
Previous Action	a_{t-1}	16
Target Joint Positions	\bar{q}	16
Tactile		
Binary Contact	c	4
Contact Pose	P	8
Contact Force Magnitude	F	4
Task		
Target Rotation Axis	\hat{k}	3

B. Privileged Information

We present the full list of privileged information (x_t) used in the simulation in table V. This is used to train the teacher with RL, and also used to obtain the target latent vector \bar{z} during student training to train the TCNN encoder. The privileged information is not used during deployment.

TABLE V: Full list of privileged information (x_t) only available in simulation.

Name	Symbol	Dimensions
Object Information		
Position	p_o	3
Orientation	r_o	4
Angular Velocity	ω_r	3
Dimensions	\dim_o	2
Center of Mass	COM_o	3
Mass	m_o	1
Gravity Vector	\hat{g}	3
Auxiliary Goal Information		
Position	p_g	3
Orientation	r_g	4

C. Reward Function

In the following, we explicitly define each term of the reward function used for multi-axis object rotation. The full reward function is:

$$r = r_{\text{rotation}} + r_{\text{contact}} + r_{\text{stable}} + r_{\text{terminate}}, \quad (4)$$

where,

$$r_{\text{rotation}} = \lambda_{\text{kp}} r_{\text{kp}} + \lambda_{\text{rot}} r_{\text{rot}} + \lambda_{\text{bonus}} r_{\text{bonus}},$$

$$r_{\text{contact}} = \lambda_{\text{rew}} (\lambda_{\text{gc}} r_{\text{gc}} + \lambda_{\text{bc}} r_{\text{bc}}),$$

$$r_{\text{stable}} = \lambda_{\text{rew}} (\lambda_{\omega} r_{\omega} + \lambda_{\text{pose}} r_{\text{pose}} + \lambda_{\text{work}} r_{\text{work}} + \lambda_{\text{torque}} r_{\text{torque}}),$$

$$r_{\text{terminate}} = \lambda_{\text{penalty}} r_{\text{penalty}}$$

Keypoint Distance Reward

$$r_{\text{kp}} = \frac{kp_{\text{dist}}}{(e^{ax} + b + e^{-ax})} \quad (5)$$

where the keypoint distance $kp_{\text{dist}} = \frac{1}{N} \sum_{i=1}^N \|k_i^o - k_i^g\|$, k^o and k^g are keypoint positions of the object and goal respectively. We use $N = 6$ keypoints placed 5 cm from the object origin in each of its principle axes, with the parameters $a = 50$, $b = 2.0$.

Rotation Reward

$$r_{\text{rot}} = \text{clip}(\Delta\Theta \cdot \hat{k}; -c_1, c_1) \quad (6)$$

The rotation reward represents the change in object rotation about the target rotation axis. We clip this reward in the limit $c_1 = 0.025\text{rad}$.

Goal Bonus Reward

$$r_{\text{bonus}} = \begin{cases} 1 & \text{if } kp_{\text{dist}} < d \\ 0 & \text{otherwise} \end{cases} \quad (7)$$

where we use kp_{dist} to represent a goal has been reached. We use $d = 0.015$ for teacher training and $d = 0.025$ for student training.

Good Contact Reward

$$r_{\text{gc}} = \begin{cases} 1 & \text{if } n_{\text{tip_contact}} \geq 2 \\ 0 & \text{otherwise} \end{cases} \quad (8)$$

where $n_{\text{tip_contact}} = \text{sum}(c)$. This rewards the agent if the number of tip contacts is greater or equal to 2 to encourage stable grasping contacts.

Bad Contact Penalty

$$r_{\text{bc}} = \begin{cases} 1 & \text{if } n_{\text{non_tip_contact}} \geq 0 \\ 0 & \text{otherwise} \end{cases} \quad (9)$$

where $n_{\text{non_tip_contact}}$ is defined as the sum of all contacts with the object that is not a fingertip. We accumulate all the contacts in the simulation to calculate this.

Angular Velocity Penalty

$$r_{\omega} = -\min(\|\omega_o\| - \omega_{\text{max}}, 0) \quad (10)$$

where the maximum angular velocity $\omega_{\text{max}} = 0.5$. This term penalises the agent if the angular velocity of the object exceeds the maximum.

Pose Penalty

$$r_{\text{pose}} = -\|q - q_0\| \quad (11)$$

where q_0 is the joint positions for some canonical grasping pose.

Work Penalty

$$r_{\text{work}} = -\tau^T \bar{q} \quad (12)$$

Torque Penalty

$$r_{\text{work}} = -\|\tau\| \quad (13)$$

where in the above τ is the torque applied to the joints during an actioned step.

Termination Penalty

$$r_{\text{terminate}} = \begin{cases} -1 & (kp_{\text{dist}} > d_{\text{max}}) \text{ or } (\hat{k}_o > \hat{k}_{\text{max}}) \\ 0 & \text{otherwise} \end{cases} \quad (14)$$

Here we define two conditions to signify the termination of an episode. The first condition represents the object falling out of grasp, for which we use the keypoint distance kp_{dist} and $d_{\text{max}} = 0.1$. The second condition represents the deviation of the local rotation axis from the target rotation axis (\hat{k}_o) beyond a maximum \hat{k}_{max} . We use $\hat{k}_{\text{max}} = 45^\circ$.

The corresponding weights for each term is: $\lambda_{\text{kp}} = 1.0$, $\lambda_{\text{rot}} = 5.0$, $\lambda_{\text{bonus}} = 10.0$, $\lambda_{\text{gc}} = 0.1$, $\lambda_{\text{bc}} = 0.2$, $\lambda_{\omega} = 0.75$, $\lambda_{\text{pose}} = 0.2$, $\lambda_{\text{work}} = 2.0$, $\lambda_{\text{torque}} = 1.0$, $\lambda_{\text{penalty}} = 50.0$.

D. Alternative Reward Formulation

We also formulate an alternative reward function consisting of an angular velocity reward and rotation axis penalty.

Angular Velocity Reward

$$r_{\text{av}} = \text{clip}(\omega \cdot \hat{k}, -c_2, c_2) \quad (15)$$

where $c_2 = 0.5$.

Rotation Axis Penalty

$$r_{\text{axis}} = 1 - \frac{\hat{k} \cdot \hat{k}_o}{\|\hat{k}\| \|\hat{k}_o\|} \quad (16)$$

where $\|\hat{k}_o\|$ is the current object axis.

We form the new r_{rotation} reward $r_{\text{rotation}} = \lambda_{\text{av}} r_{\text{av}} + \lambda_{\text{rot}} r_{\text{rot}}$. We provide an additional object axis penalty $\lambda_{\text{axis}} r_{\text{axis}}$ in the r_{stable} term and remove the angular velocity penalty, $\lambda_{\omega} = 0$. The weights are $\lambda_{\text{av}} = 1.5$ and $\lambda_{\text{axis}} = 1.0$. We keep all other terms of the reward function the same.

E. Grasp Generation

To generate stable grasps, we initiate the object at 13cm above the base of the hand at random orientations and initialize the hand at a canonical grasp pose at the palm-up hand orientation. We then sample relative offset to the joint positions $\mathcal{U}(-0.3, 0.3)\text{rad}$. We run the simulation by 120 steps (6s) while sequentially changing the gravity direction from 6 principle axes of the hand ($\pm xyz$ -axes). We save the object orientation and joint positions (10000 grasp poses per object) if the following conditions are satisfied:

- The number of tip contacts is greater than 2.
- The number of non-tip contacts is zero
- Total fingertip to object distance is less than 0.2
- Object remains stable for the duration of the episode.

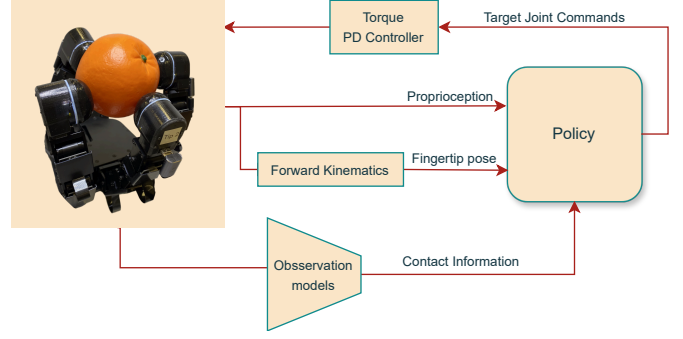


Fig. 9: Real-world robot hand control pipeline.

TABLE VI: Policy training parameters. Please refer to ref. [38] and [29] for a detailed explanation of each hyperparameter.

Teacher	
MLP Input Dim	18
MLP Hidden Units	[256, 128, 8]
MLP Activation	ReLU
Policy Hidden Units	[512, 256, 128]
Policy Activation	ELU
Learning Rate	5×10^{-3}
Num Envs	8192
Horizon Length	8
Minibatch Size	32768
Num Mini Epochs	5
Discount	0.99
GAE τ	0.95
Advantage Clip ϵ	0.2
KL Threshold	0.02
Gradient Norm	1.0
Optimizer	Adam
Student	
TConv Input Dim	[30, N]
TConv Hidden Units	[N, N]
TConv Filters	[N, N, N]
TConv Kernel	[9, 5, 5]
TConv Stride	[2, 1, 1]
TConv Activation	ReLU
Latent Vector Dim z	8
Policy Hidden Units	[512, 256, 128]
Policy Activation	ELU
Learning Rate	3×10^{-4}
Num Envs	8192
Batch Size	8192
Num Mini Epochs	1
Optimizer	Adam

F. Domain Randomization

In addition to the initial grasping pose, target rotation axis and hand orientation, we also include additional domain randomization during teacher and student training to improve sim-to-real performance, shown in table VII.

TABLE VII: Domain randomization parameters.

Object	
Capsule Radius (m)	[0.025, 0.034]
Capsule Width (m)	[0.000, 0.012]
Box Width (m)	[0.045, 0.06]
Box Height (m)	[0.045, 0.06]
Mass (kg)	[0.025, 0.20]
Object: Friction	10.0
Hand: Friction	10.0
Center of Mass (m)	[-0.01, 0.01]
Disturbance: Scale	2.0
Disturbance: Probability	0.25
Disturbance: Decay	0.99
Hand	
PD Controller: Stiffness	$\times \mathcal{U}(0.9, 1.1)$
PD Controller: Damping	$\times \mathcal{U}(0.9, 1.1)$
Observation: Joint Noise	0.03
Observation: Fingertip Position Noise	0.005
Observation: Fingertip Orientation Noise	0.01
Tactile	
Observation: Pose Noise	0.0174 rad
Observation: Force Noise	0.1

G. System Identification

To reduce the sim-to-real gap of the allegro hand, we perform system identification to match the simulated robot hand with the real world. We model each of the 16 DoF of the hand with the parameters; stiffness, damping, mass, friction, and armature, resulting in a total of 80 parameters to optimize. We collect corresponding trajectories in simulation and the real world in various hand directions and use an optimizer to minimize the mean-squared error of the trajectories to find the best matching simulation parameters.

H. Simulated Tactile Processing

To simulate our soft tactile sensor in a rigid body simulator, we process the received contact information from the simulator to make up the tactile observations. To simulate the elastic deformation of the soft tip in the real world when force is applied, we apply an exponential average on the contact force obtained in simulation.

$$\mathbf{F} = \alpha F_t + (1 - \alpha) F_{t-1} \quad (17)$$

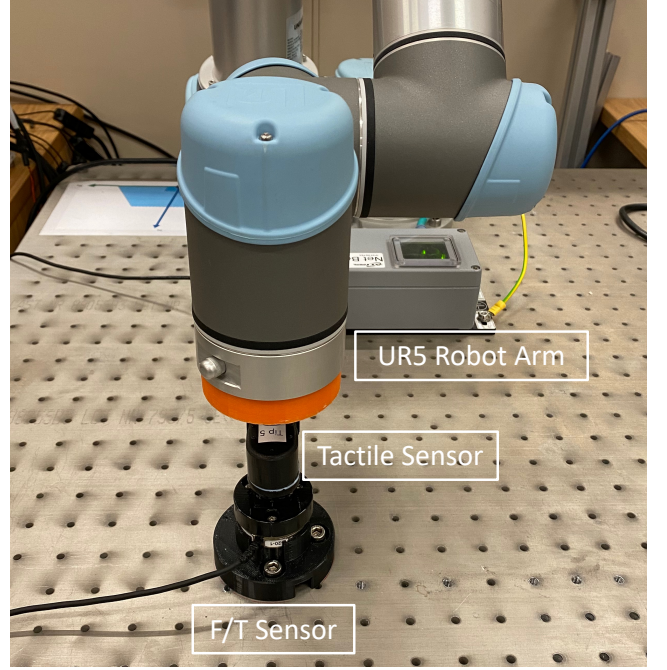
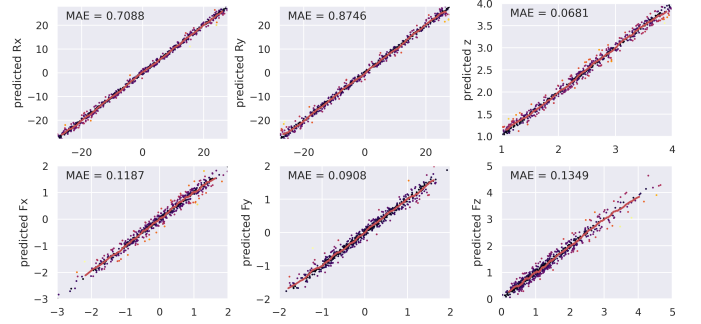
where we use $\alpha = 0.5$. We then apply a saturation limit and re-scaling to align simulated force limits with the real force limits.

$$\mathbf{F} = \beta_F \text{clip}(F, F_{\min}, F_{\max}) \quad (18)$$

where we use $\beta_F = 0.6$, $F_{\min} = 0.0\text{N}$, $F_{\max} = 5.0\text{N}$. We also apply the same saturation and rescaling function for the contact pose.

$$\mathbf{P} = \beta_P \text{clip}(P, P_{\min}, P_{\max}) \quad (19)$$

where we use $\beta_P = 0.6$, $P_{\min} = -0.53\text{rad}$, $P_{\max} = 0.53\text{rad}$.

**Fig. 10:** Data collection setup for training observation model, including an F/T sensor and a UR5 Robot arm.**Fig. 11:** Error plots on test data for a sample observation model.

I. Policy Details

The network architecture and training hyperparameters are shown in table VI. The proprioception policy uses an observation input dim of $N = 79$, the binary touch $N = 83$, and the full touch $N = 95$. We use a history of 30 time steps as input to the TConv and encode the privileged information into a latent vector of size=8 for all the policies.

J. Tactile Data Collection

The data collection setup for tactile feature extraction is shown in (shown in Fig. 10). We collect data by tapping the sensor on a flat stimulus fixed onto a force torque sensor. In order to capture sufficient contact features needed for the in-hand object rotation task, we sample the sensor poses with the ranges shown in VIII.

K. Tactile Image Processing

The tactile sensors provide raw RGB images from the camera module. We use an exposure setting of 312.5 and a resolution of 640×480 , providing a frame rate of up to 30

TABLE VIII: Sensor pose sampling ranges used during tactile data collection for training the pose and force prediction models, relative to the sensor coordinate frame.

Pose Component	Sampled range
Depth z (mm)	[-1, -4]
Shear S_x (mm)	[-2, -2]
Shear S_y (mm)	[-2, -2]
Rotation R_x (deg)	[-28, 28]
Rotation R_y (deg)	[-28, 28]

TABLE IX: Observation model training parameters.

Observation Model	
Conv Input Dim	[240, 135]
Conv Filters	[32, 32, 32, 32]
Conv Kernel	[11, 9, 7, 5]
Conv Stride	[1, 1, 1, 1]
Max Pooling Kernel	[2, 2, 2, 2]
Max Pooling Stride	[2, 2, 2, 2]
Output Dim	6
Batch Normalization	True
Activation	<i>ReLU</i>
Learning Rate	1×10^{-4}
Batch Size	16
Num Epochs	100
Optimizer	Adam

FPS. The images are then postprocessed to compute tactile observations. For all tactile observations, we convert the raw image to greyscale and rescale the dimension to 240×135 .

Binary Contact: We further apply a medium blur filter with an aperture linear size of 11, followed by an adaptive threshold with a block size of 55 pixels and a constant offset value of -2. These operations improve the smoothness of the image and filter out unwanted noise. The postprocessed image is compared with a reference image using the Structural Similarity Index (SSIM) to compute binary contact (0 or 1). We use an SSIM threshold of 0.6 for contact detection.

Contact Pose and Force: We directly use the resized greyscale image for contact force and pose prediction. Table IX shows the CNN model architecture and training hyperparameters. During data collection, we collect 6 labels for training: contact depth z , contact pose in R_x , contact pose in R_y , and contact forces F_x , F_y and F_z . For each fingertip sensor, we collect 3000 images (2400 train and 600 test) and train separate models. The prediction error for test data for one of the sensors is shown in Fig. 11. From the target labels, we only use contact pose R_x , R_y and contact force F_x , F_y , F_z to compute the tactile observations.

L. Ablation Experiments

We provide additional ablation studies to analyze the design choices for our goal formulation. The effect of goal update tolerance d for the student training and the goal update increment intervals are shown in table XI. The policies are

TABLE X: Dimensions and mass of real-world object set consisting of plastic fruits and everyday objects.

Real-world Object Set		
	Dimensions (mm)	Mass (g)
Plastic Apple	$75 \times 75 \times 70$	60
Plastic Orange	$70 \times 72 \times 72$	52
Plastic Pepper	$61 \times 68 \times 65$	10
Plastic Peach	$62 \times 56 \times 55$	30
Plastic Lemon	$52 \times 52 \times 65$	33
Tin Cylinder	$45 \times 45 \times 63$	30
Cube	$51 \times 51 \times 51$	65
Gum Box	$90 \times 80 \times 76$	89
Container	$90 \times 80 \times 76$	32
Rubber Toy	$80 \times 53 \times 48$	27

TABLE XI: We compare the performance of policies trained with different design choices in the goal formulation. We compare goal update tolerance and goal increment intervals and provide metrics for average successive goals reached, rotation count (Rot), and time to terminate (TTT).

Goal Update	Rot	TTT(s)	#Success
$d = 0.15$	0.75	28.1	3.07
$d = 0.20$	1.36	27.7	4.48
$d = 0.25$	1.77	27.2	5.26
Goal Increment Interval	Rot	TTT(s)	#Success
$\theta = 50^\circ$	1.30	27.1	3.86
$\theta = 40^\circ$	1.50	26.7	4.36
$\theta = 30^\circ$	1.77	27.2	5.26

trained with different design choices but fixed during testing ($d = 0.25$ and interval $\theta = 30^\circ$).

The performance can be significantly affected by the goal update tolerance. As the tolerance reduced during student training, the number of average rotations and successive goals reached per episode was lower. This suggests that the performance of the teacher policy was poorly transferred and the student could not learn the object rotation skill effectively. Increasing the goal increment intervals also resulted in fewer object rotations achieved.